

## Selecting Annealing Temperature of P3HT/PCBM Incorporated with Nano-diamonds Using Thermal Desorption Spectroscopy

Shang-Chou Chang<sup>1,\*</sup>, Yu-Jen Hsiao<sup>2</sup>, To-Sing Li<sup>1</sup>

<sup>1</sup> Department of Electrical Engineering, Kun Shan University, Tainan City 71010, Taiwan

<sup>2</sup> National Nano Device Laboratories, Tainan City 74147, Taiwan

\*E-mail: [jchang@mail.ksu.edu.tw](mailto:jchang@mail.ksu.edu.tw)

Received: 10 November 2014 / Accepted: 4 December 2014 / Published: 30 December 2014

---

This work reports a novel method to determine the annealing temperature of blended poly (3-hexylthiophene) and [6,6]-phenyl C<sub>61</sub> butyric acid methyl ester ( P3HT/PCBM ) with nano-diamonds (ND) (P3HT/PCBM /ND) based organic solar cells (OSC). The P3HT/PCBM /ND with 4 wt% ND doping (P3HT/PCBM /4 wt% ND ) based OSC demonstrate highest power conversion efficiency compared with those having other ND doping concentrations. Thermal desorption spectra of unannealed P3HT/PCBM /4 wt% ND show two desorption peaks from all desorption species at around 130 and 185°C. The two temperatures are close to the glass transition temperature of PCBM and melting temperature of P3HT, respectively. The P3HT/PCBM /4 wt% ND were annealed at different temperatures (unannealed, 120, 140, 175 and 195°C, respectively) to fabricate OSC, and their photovoltaic characteristics were explored. Measured results indicate the desorption peak at 130°C corresponds to not only an activated state related with the glass transition temperature of PCBM but also a turning point in P3HT/PCBM/4 wt% ND. External quantum efficiency and power conversion efficiency of the P3HT/PCBM /4 wt% ND based OSC increase from unannealed condition to annealed at 120°C, and deteriorate when the annealing temperature is higher than 120°C. It can be attributed to relatively good crystallinity in both P3HT and PCBM for OSC annealed at 120°C.

---

**Keywords:** annealing temperature, nano-diamonds, P3HT/PCBM, organic solar cell

### 1. INTRODUCTION

Organic solar cells (OSC) offer numerous advantages such as low-cost fabrication, large-area capability and physical flexibility. Bulk heterojunction solar cells are usually made by blending *p*-type conjugated polymers with *n*-type conjugated polymers, fullerenes, fullerene derivatives or nanoparticles and they are constructed with a network of nano-sized area between electron donor and

electron acceptor in OSC [1-4]. The *p*-type conjugated polymers with fullerene derivatives such as poly (3-hexylthiophene) (P3HT) and [6,6]-phenyl C<sub>61</sub> butyric acid methyl ester (PCBM) blend (P3HT/PCBM) have been intensively investigated [5-6]. Nanocrystals like nano-diamonds (ND), cadmium selenide, silicon and zinc oxide doped hybrid solar cells have been reported due to their promising photovoltaic properties [7-10]. Nanocrystals have advantages in solar cell materials due to high surface to volume ratio, quantum confinement and quantum size effect [11-12]. Nontoxicity, strong ultraviolet absorption (energy band gap ~5.4–5.6 eV) and high thermal conductivity make ND a prime candidate in hybrid solar cells [7].

Thermal annealing can provide positive effects on photovoltaic process of P3HT/PCBM based OSC. Positive effects are such as improving surface morphology and crystallinity of photoactive materials, contact resistance between active materials and electrode to facilitate charge generation, transport and collection [13]. However, thermal annealing can also bring negative effects on photovoltaic process of P3HT/PCBM based OSC if thermal annealing is too much. Negative effects are such as PCBM aggregation, phase separation between P3HT and PCBM to reduce power conversion efficiency (PCE) [14]. Annealing temperature of P3HT/PCBM is therefore selected as high as possible to increase positive effects, but not higher than a turning temperature which the net effects become negative. Selecting annealing temperature is one of the key factors in improving short circuit current density ( $J_{sc}$ ), open circuit voltage ( $V_{oc}$ ) and PCE [15].

The technique of thermal desorption spectroscopy (TDS) is to heat samples in vacuum and measure the desorbed species from the heated samples. It has been used in studying metal or gas desorption behavior, thermal stability, catalyst reaction and hydrogen storage [16-19]. Our group has recently applied TDS to investigate the thermal effect on fluorine doped zinc oxide and aluminum doped zinc oxide films [20-21]. This work applied TDS to evaluate the annealing temperature of ND doped P3HT/PCBM (P3HT/PCBM/ND). The unannealed P3HT/PCBM/ND with different ND doping concentrations based OSC were produced in the beginning. The P3HT/PCBM/ND with 4 wt% ND (P3HT/PCBM/4 wt% ND) based OSC has highest PCE compared to others. The TDS of P3HT/PCBM/4 wt% ND shows two desorption peaks at around 130 °C and 185 °C for all desorption species. A desorption peak in TDS corresponds to an activation energy of desorption [20], which corresponds to an activated state in the measured sample. Two desorption peaks at around 130 °C and 185 °C correspond two activated states in P3HT/PCBM/4 wt% ND. One of the two activated states could be also a turning point for the photovoltaic characteristics of P3HT/PCBM/4 wt% ND based OSC. Annealing temperature higher than 130 °C or 185 °C for P3HT/PCBM/4 wt% ND could make the photovoltaic characteristics of P3HT/PCBM/4 wt% ND based OSC negative instead of positive. The P3HT/PCBM/4 wt% ND were annealed at 10 °C lower or higher than the 130 or 185 °C (120, 140, 175 and 195 °C, respectively). Results on photovoltaic characteristics of P3HT/PCBM/4 wt% ND annealed at different annealing temperatures based OSC imply 130 °C corresponds to not only an activated state related with the glass transition temperature of PCBM but also a turning point in P3HT/PCBM/4 wt% ND.

## 2. EXPERIMENTS

The hybrid OSC were fabricated on indium tin oxide (ITO)-coated glass substrates. Patterned ITO substrates were oxygen plasma treated in a reactive ion etching tool to increase hydrophilic property of the ITO surface. A layer of poly(3,4-ethylenedioxythiophene)/poly(styrenesulfonate) (PEDOT:PSS, CLEVIOS™ P VP AI 4083, Heraeus Clevios GmbH, Leverkusen, Germany) about 40 nm thick was spin-coated on the ITO substrate and baked at 120 °C for 30 min. The active layer consisted of P3HT (RMI-001E, Rieke Met. Inc., Lincoln, Nebraska, USA) and PCBM ([60]PCBM, Nano-C, Westwood, Maryland, USA) in 10:8 wt % ratio dissolved in 1,2-dichlorobenzene with 0, 2, 4, 6 and 8 wt % ND, respectively. The ND were produced by the detonation method.

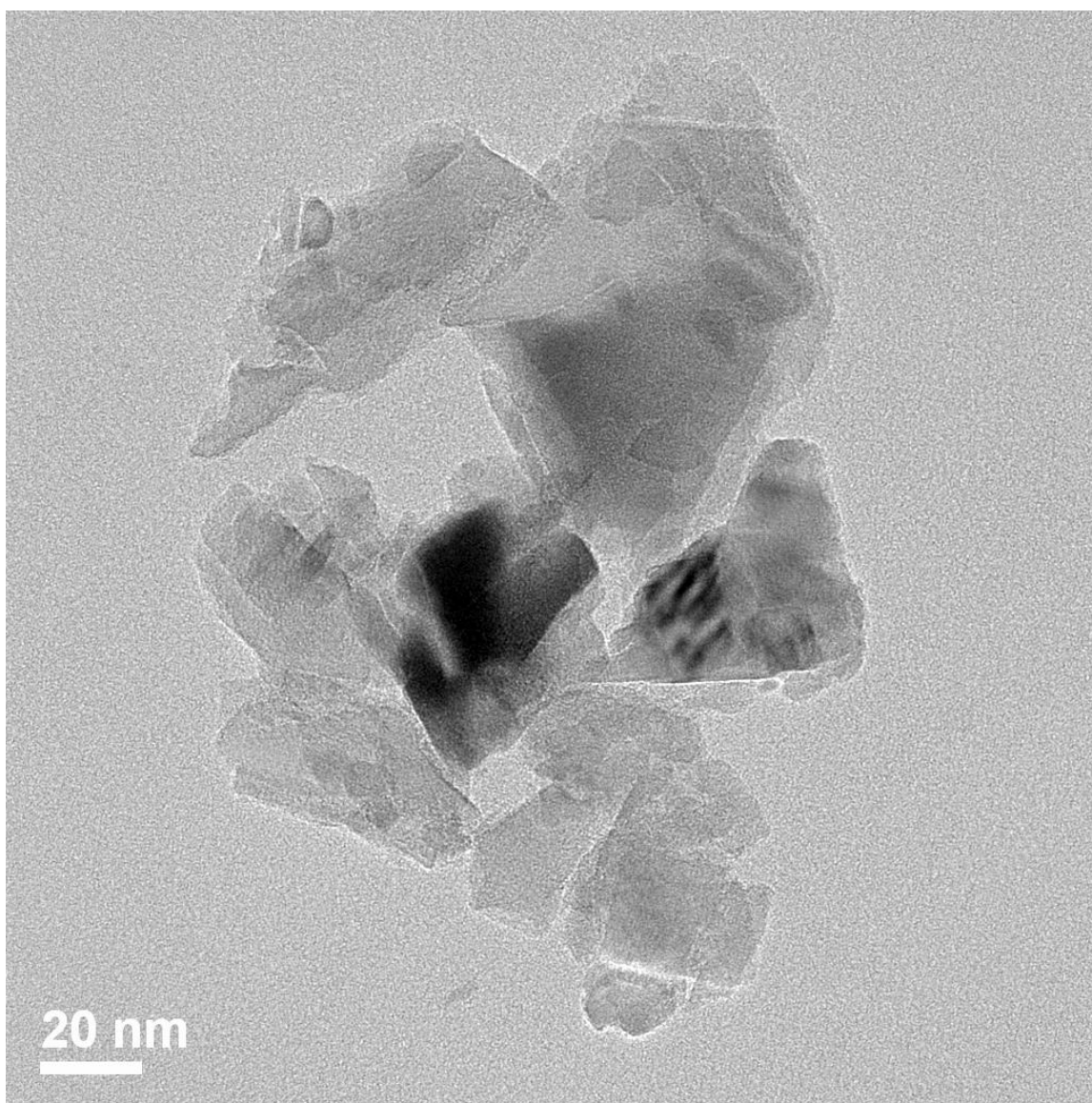


**Figure 1.** Transmission electron microscopy image of ND in P3HT/PCBM/ND hybrid films with an average diameter of 100 nm.

Figure 1 shows the transmission electron microscopy (TEM) image of ND in P3HT/PCBM/ND hybrid films with an average diameter of 100 nm. The photoactive materials were spin coated with rotation speed of 800 rpm in a glove box, and the resulting film was about 300 nm in thickness. A Ca/Al electrode with 120 nm in thickness was then deposited onto the active layer through a shadow mask by using thermal evaporation. The device structure of the produced OSC, in which P3HT/PCBM/ND is the photoactive layer of the device, was shown in figure 2a.

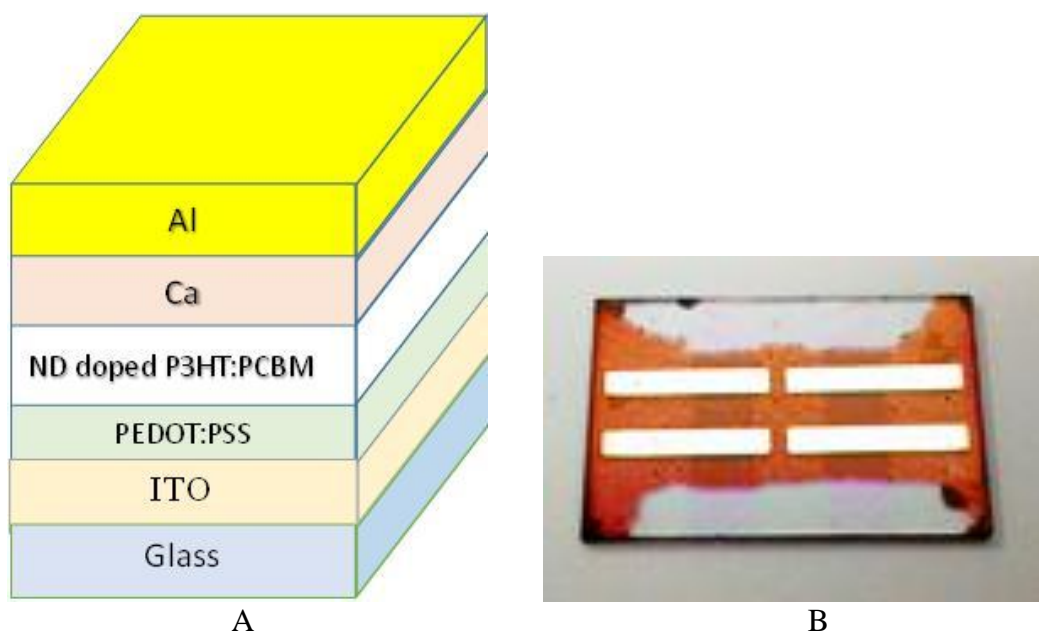


**Figure 2.** (a) The device structure of the P3HT/PCBM/ND based OSC. (b) The photograph of processed organic solar cell.

The actual organic solar cell device was shown in figure 2b and the device area was about  $0.04 \text{ cm}^2$ . The optical absorption spectra were obtained by using an optical spectrometer (U-4100, Hitachi, Minato-ku, Tokyo Japan), and current–voltage measurements were obtained by using a source meter (2410, Keithley, Cleveland, Ohio, USA), and a solar simulator (Sun 3000 class AAA, TELTEC, Hong Kong) with the AM 1.5 filter under an irradiation intensity of  $100 \text{ mW cm}^{-2}$ . The P3HT/PCBM/4 wt% ND shows the highest PCE among P3HT/PCBM/ND with different ND doping concentrations based OSC.

The TDS of unannealed P3HT/PCBM/4 wt% ND films were measured. The measurement system of TDS was pumped down to  $10^{-7}$  Torr range or below. Then, the measured films were linearly heated by a proportional-integral-derivative controller at a fixed  $10^\circ\text{C}$  per minute from RT to  $300^\circ\text{C}$ . The heating of the measurement system was closed after the measured films reached  $300^\circ\text{C}$ . The temperature of the TDS measurement system was naturally cooled down in vacuum. Apparent ion currents corresponding to ion mass to charge ratio ( $m/e$ ) 18, 44 and 56 were measured with a quadruple mass spectrometer (QMS). Two desorption peaks in TDS were observed at around  $130$  and  $185^\circ\text{C}$  for all desorption species. The annealing temperature of P3HT/PCBM/4 wt %ND films was selected at  $120$ ,  $140$ ,  $175$  and  $195^\circ\text{C}$  respectively ( $10^\circ\text{C}$  lower or higher than the corresponding temperatures of

two desorption peaks ). Optical absorption spectra and photovoltaic properties of P3HT/PCBM/4 wt% ND annealed at different annealing temperatures based OSC were measured and compared.

### 3. RESULTS AND DISCUSSION

The current density-voltage ( $J-V$ ) characteristics of the OSC made of unannealed P3HT/PCBM/ND with different ND doping concentrations were measured under  $100 \text{ mW/cm}^2$  in illumination intensity shown in Figure 3. The photovoltaic characteristics of samples doped with different ND doping concentrations are given in table 1.

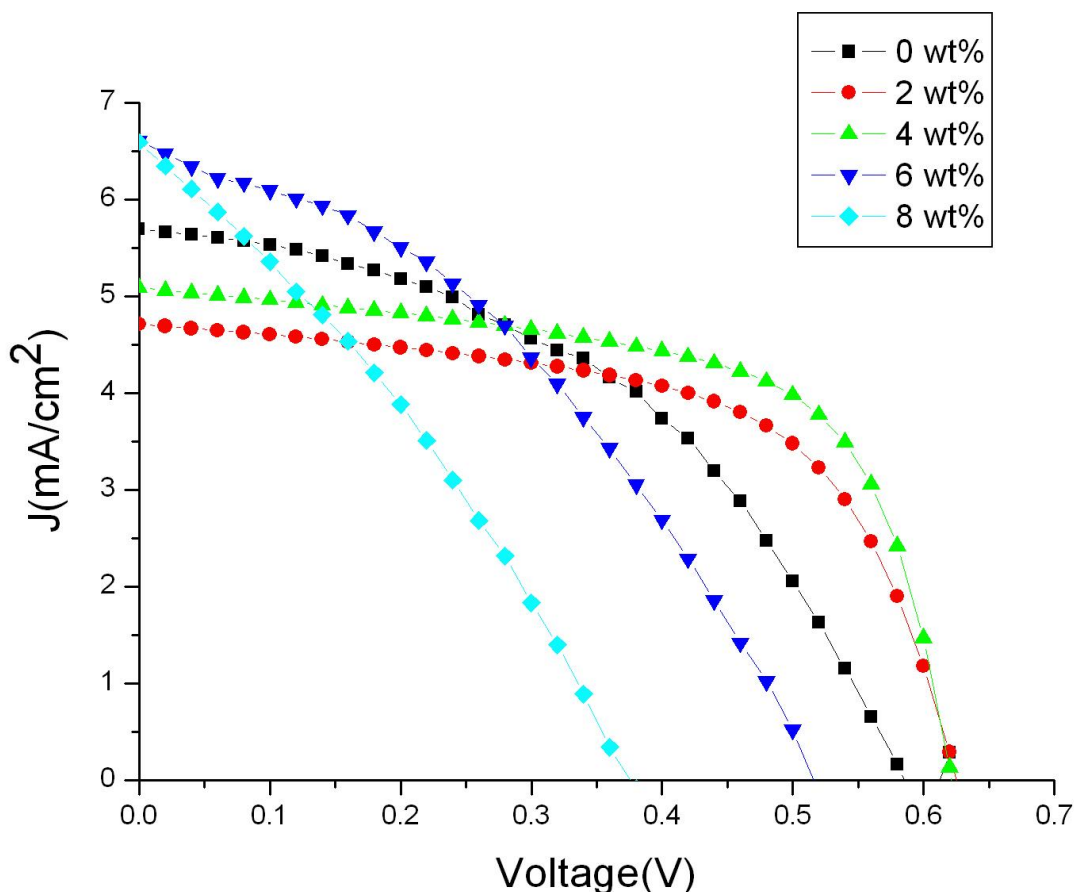


**Figure 3.** The current density-voltage ( $J-V$ ) characteristics of the OSC made of unannealed P3HT/PCBM/ND with various ND concentration.

The PCE in OSC rise from 1.53 to 1.99% with ND doping concentration till 4 wt%. The ND doping increases the donor/acceptor interface area for charge separation and shortens the electron transfer path in P3HT/PCBM. With thermal annealing,  $V_{oc}$  and FF have similar values for OSC made of the same nanocrystals doped P3HT/PCBM but with different doping concentration reported on nanocrystals doped P3HT/PCBM from previous literatures [7-9]; without annealing,  $V_{oc}$  and FF have apparent different values for OSC made of P3HT/PCBM/ND with different ND doping concentrations shown in table 1.  $V_{oc}$  is determined by energy level difference between the component materials in

OSC [22]. FF relates with recombination of photo-generated charge carriers during photovoltaic process [22].

**Table 1.** Photovoltaic performance of unannealed P3HT/PCBM/ND with different ND doping concentrations.

ND concentration (wt%)	V <sub>oc</sub> (V)	J <sub>sc</sub> (mA/cm <sup>2</sup> )	FF (%)	PCE (%)
0	0.59	5.69	44.6	1.53
2	0.61	4.71	60.2	1.76
4	0.61	5.09	63.1	1.99
6	0.52	6.59	38.3	1.32
8	0.38	6.59	30.9	0.78

Thermal annealing improves nanoscale morphology and crystallinity of photoactive layer. Morphology and crystallinity of photoactive layer have direct influence on V<sub>oc</sub> and FF. Unannealed P3HT/PCBM/ND with different ND doping concentrations have different morphology and crystallinity and therefore V<sub>oc</sub> and FF have different values.

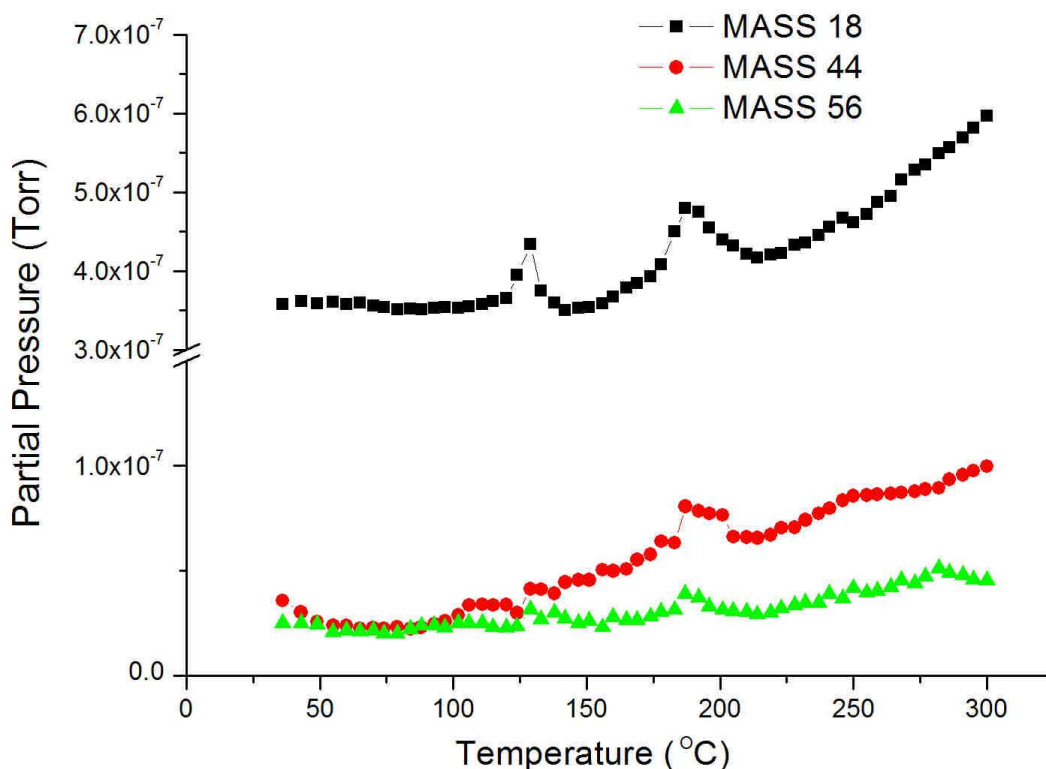


**Figure 4.** The thermal desorption spectroscopy of unannealed P3HT/PCBM/4 wt% ND films.

The TDS of unannealed P3HT/PCBM/4 wt %ND films was shown in figure 4. Three desorption species apparently found from QMS corresponding to ion mass to charge ratio ( $m/e$ ) 18, 44 and 56 were displayed. The species for  $m/e=18$  attributes water vapor. Desorption intensity of water vapor is several times higher than that of the other two species. The measured samples contain PEDOT/PSS and PCBM which are significantly hygroscopic [23-24]. These may explain high desorption intensity of water vapor from measured samples even though all samples were processed in a water-vapor-controlled glove box. All three desorption species have similar two desorption peaks at around 130 °C and 185 °C in figure 4. The two temperatures are close to the reported glass transition temperature of PCBM (131.2 °C) and melting temperature of P3HT (178 °C) [25-26]. The two desorption peaks in figure 4 therefore attribute to two activated states related with glass transition temperature of PCBM and melting temperature of P3HT in P3HT/PCBM/4 wt %ND.

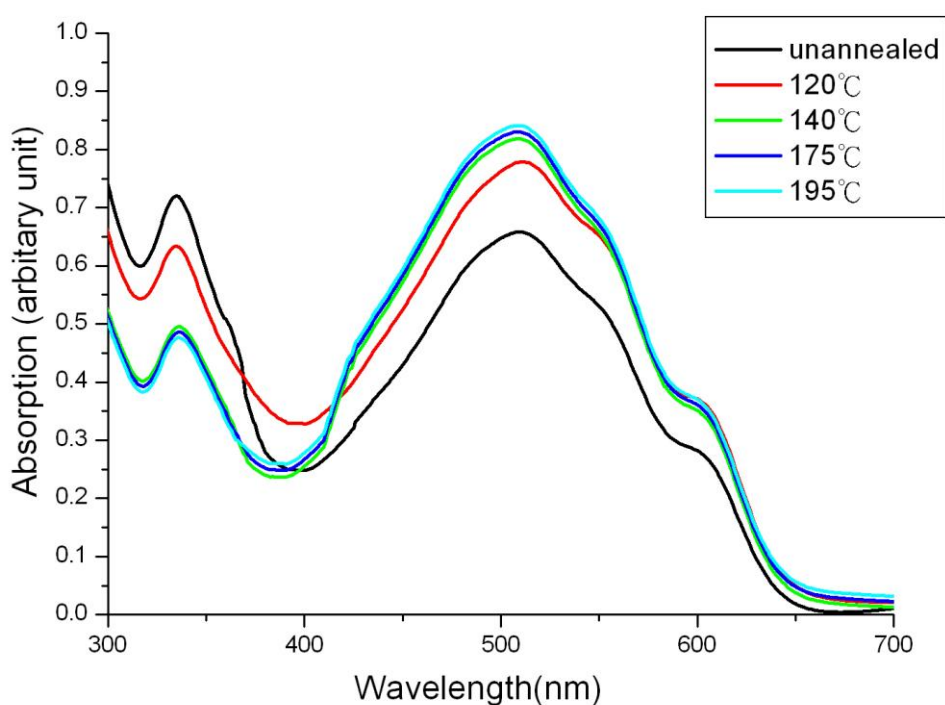


**Figure 5.** Optical absorption spectra of P3HT/PCBM/4 wt% ND annealed at different annealing temperatures (unannealed, 120, 140, 175 and 195 °C)

Optical absorption spectra of P3HT/PCBM/4 wt% ND annealed at different annealing temperatures (unannealed, 120, 140, 175 and 195 °C) were shown in figure 5. Two absorption peaks were found in figure 5. The peak located at 300-400 nm attributes to PCBM and its intensity decreases with annealing temperature when the annealing temperature is up to 140 °C. However, the other peak located at 500-600 nm attributes to P3HT and its intensity increases with annealing temperature when the annealing temperature is up to 140 °C. The intensities of two peaks are similar to P3HT/PCBM/4 wt% ND annealed at 140, 175 and 195 °C. The intensity of optical absorption strongly relates with crystallization of photoactive materials [27]. PCBM crystallizes more readily and faster compared to P3HT, and forms homogeneous crystals at room temperature [27].

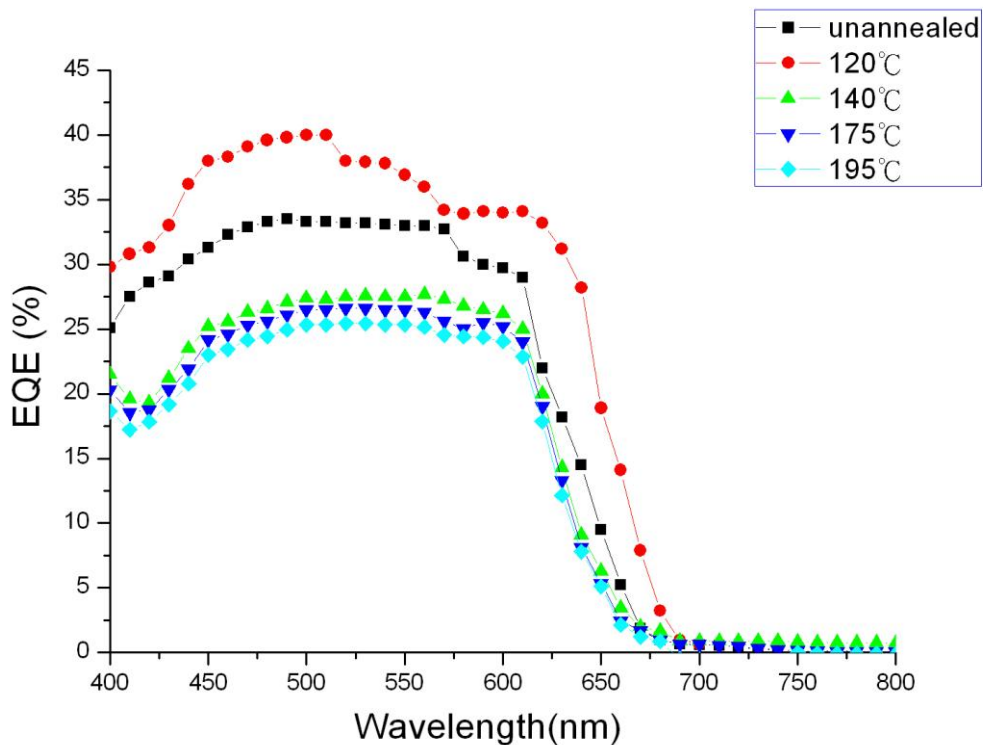


**Figure 6.** External quantum efficiency spectra of the P3HT/PCBM/4 wt% ND based OSC annealed at different annealing temperatures (unannealed, 120, 140, 175 and 195°C)

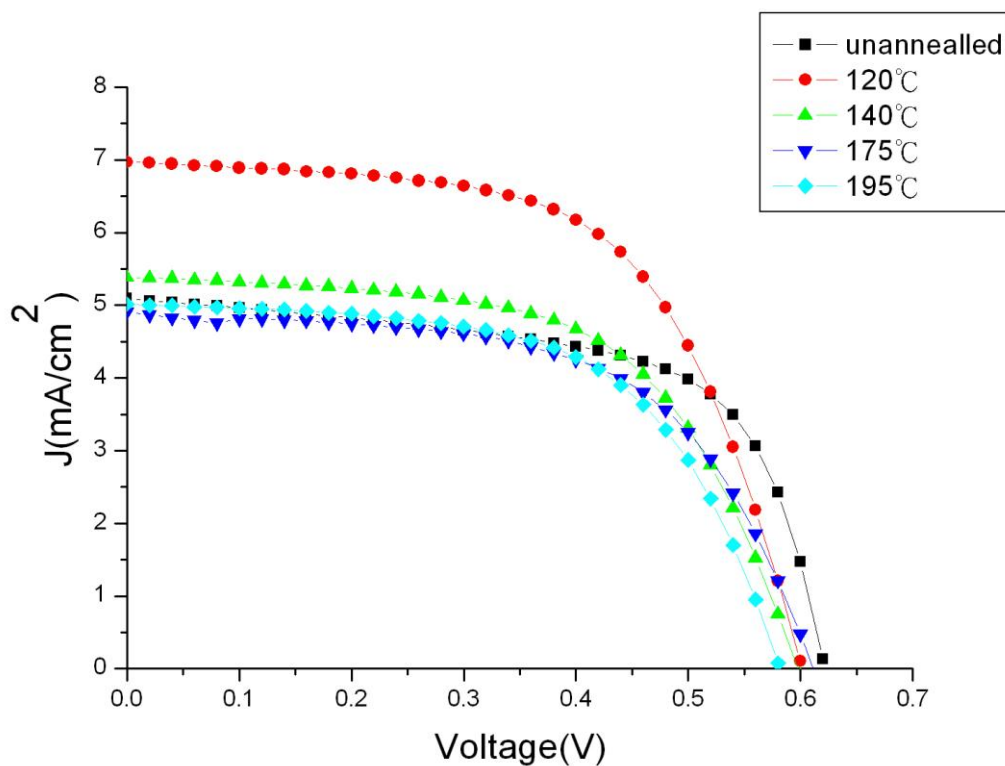


**Figure 7.** Current density-voltage ( $J-V$ ) characteristics and photovoltaic characteristics of the P3HT/PCBM/4 wt% ND based OSC annealed at different annealing temperatures (unannealed, 120, 140, 175 and 195°C)

**Table 2.** Photovoltaic characteristics of the P3HT/PCBM/ 4 wt% ND based OSC annealed at different annealing temperatures (unannealed, 120, 140, 175 and 195°C)

Annealing Temperature (°C)	V <sub>oc</sub> (V)	J <sub>sc</sub> (mA/cm <sup>2</sup> )	FF (%)	PCE (%)
unannealed	0.61	5.09	63.1	1.99
120	0.60	6.97	60.3	2.52
140	0.60	5.38	58.8	1.90
175	0.61	4.73	63.3	1.82
195	0.56	5.05	60.3	1.73

Annealing process was found to increase the crystallization of P3HT and the segregation of PCBM in P3HT/PCBM. Upon annealing, PCBM segregates and forms disjointed clusters of islands as its crystals begin to break-up especially when the annealing temperature is higher than the glass transition temperature of PCBM (the temperature corresponding to the first desorption peak in TDS of P3HT/PCBM/4 wt %ND). Small molecules of the segregated PCBM diffuse into the P3HT matrix allowing the latter to re-organize itself into stacks and long chains as a result increasing the crystallization [28].

External quantum efficiency (EQE) spectra of the P3HT/PCBM/4 wt %ND based OSC annealed at different annealing temperatures (unannealed, 120, 140, 175 and 195°C) were shown in figure 6. The magnitude of EQE is similar to annealing temperature higher than 120°C (140, 175 and 195°C). The magnitude sequence of EQE value at the same wavelength for OSC in figure 6 is 120°C > unannealed > over 120°C (140, 175 and 195°C). Current density-voltage (*J-V*) characteristics and photovoltaic characteristics of the P3HT/PCBM/4 wt %ND based OSC annealed at different annealing temperatures were shown in figure 7 and table 2, respectively.

The magnitude sequence of PCE for OSC in table 2 is the same as that of EQE value at the same wavelength in figure 6 (120°C > unannealed > over 120°C (140, 175 and 195°C)). The first desorption peak at 130°C in figure 4 corresponds to not only an activated state but also a turning point in P3HT/PCBM/4 wt %ND based on results of optical absorption, EQE and PCE. The EQE and PCE of P3HT/PCBM/4 wt %ND increase from an unannealed condition to annealed at 120°C, and apparently deteriorate when the annealing temperature is higher than 130°C (140, 175 and 195°C). The turning point of P3HT/PCBM/4 wt %ND corresponds to glass transition temperature of PCBM. Results on EQE and photovoltaic characteristics in figure 6 and table 1 can be explained with results on optical absorption in figure 5. Crystallization of both P3HT and PCBM is important for photovoltaic characteristics of the P3HT/PCBM/4 wt %ND based OSC. Photo-generated charge carriers need good crystallization in photoactive layer to provide easy transport pathways during photovoltaic process. Annealing at 120°C which is close but lower than a turning point :130°C can make both P3HT and PCBM in P3HT/PCBM/4 wt %ND have relatively good crystallization observed from absorption intensity in figure 5. The unannealed condition for P3HT/PCBM/4 wt% ND has poor crystallization for P3HT. The annealing temperature higher than 120°C for P3HT/PCBM/4 wt% ND has poor crystallization for PCBM. Good crystallization of both P3HT and PCBM makes charge

carriers easily transport in photoactive layer. The  $J_{sc}$  and PCE of the 120°C- annealed OSC is therefore highest compared to others in table 2.

#### 4. CONCLUSIONS

Photovoltaic characteristics of OSC for unannealed P3HT/PCBM/ND with different ND doping concentrations indicate P3HT/PCBM/4 wt %ND based OSC has highest PCE. Results on TDS of P3HT/PCBM/4 wt %ND show three desorption species. The major desorption species is attributed as water vapor. Two desorption peaks at 130 and 185°C from all desorption species were found. The two temperatures are close to the glass transition temperature of PCBM and melting temperature of P3HT, respectively. The first desorption peak at 130°C corresponds to not only an activated state but also a turning point in P3HT/PCBM/4 wt %ND. EQE and PCE of P3HT/PCBM/4 wt %ND based OSC increase from unannealed condition to annealed at 120°C, and apparently deteriorate when the annealing temperature is higher than 120°C. The P3HT/PCBM/4 wt %ND based OSC can obtain 2.52% in PCE with annealing at 120°C. Annealing at 120°C for P3HT/PCBM/4 wt %ND can make both P3HT and PCBM have relatively good crystallization. Good crystallization of both P3HT and PCBM makes charge carriers easily transport in P3HT/PCBM/4 wt %ND based OSC.

#### ACKNOWLEDGEMENTS

The authors would like to thank the National Science Council of Taiwan for financially supporting this research under grant NSC 102-2221-E-168 -037 – and Kai-Yu Chang for carrying out part of measurements.

#### References

1. S. Günes, H. Neugebauer, and N. S. Sariciftci, *Chemical Reviews*, 107(4)(2007)1324.
2. P.V. Kamat, *The Journal of Physical Chemistry C*, 111(2007)2834.
3. P.V. Kamat, *The Journal of Physical Chemistry C*, 112(2008)18737.
4. B.R. Saunders and M.L. Turner, *Advances in Colloid and Interface Science*, 138(2008)1.
5. S.W. Lee, H.J. Lee, J.H. Choi, W.G. Koh, J.M. Myoung, J.H. Hur, J.J. Park, J.H. Cho and U. Jeong, *Nano Letters*, 10(2010)347.
6. G. Li, V. Shrotriya, J.S. Huang, Y. Yao, T. Moriarty, K. Emery and Y. Yang, *Nature Materials*, 4(11)(2005)864.
7. Y. Hsiao, T. Fang, L. Ji, Y. Lee, and B. Dai, *Electrochemistry Communications*, 18(1)(2012)4.
8. S.C. Chang, Y.J. Hsiao, and T.S. Li, *Journal of Electronic Materials*, 43(9)(2014)3077.
9. S.C. Chang, Y.J. Hsiao, and T.S. Li, *Journal of Nanomaterials*, 2013(2013)Article ID 354035.
10. S. V. Bhat, A. Govindaraj, and C. N. R. Rao, *Solar Energy Materials and Solar Cells*, 95(8)(2011)2318.
11. S. Q. Feng, D. P. Yu, H. Z. Zhang, Z. G. Bai, and Y. Ding, *Journal of Crystal Growth*, 209(2-3)(2000)51.
12. A. C. Varonides, *Renewable Energy*, 33(2)(2008)273.
13. Y. Zhou, F. S. Riehle, Y. Yuan, H. Schleiermacher, M. Niggemann, G. A. Urban, and M. Krüger, *Applied Physics Letters*, 96(2010)013304.

14. M. J. Greaney, S. Das, D. H. Webber, S. E. Bradforth, and R. L. Brutchey, *ACS NANO*, 6(2012)4222.
15. J. Albero, P. Riente, J. N. Clifford, M. A. Pericàs, and E. Palomares, *The Journal of Physical Chemistry C*, 117(2013)13374.
16. D. A. King, *Surface Science*, 47(1)(1975)384.
17. B. Hokkanen, S. Funk, U. Burghaus, A. Ghicov, and P. Schmuki, *Surface Science*, 601(19)(2007)4620.
18. K. Higuchia, K. Yamamoto, H. Kajioka, K. Toiyama, M. Honda, S. Orimo and H. Fujii, *Journal of Alloys and Compounds*, 330–332(2002)526.
19. N. Patel, A. Kale, P. Mosaner, R. Checchetto, A. Miotello, and G. Das, *Renewable Energy*, 33(2)(2008)232.
20. S. C. Chang, T. C. Lin, T. S. Li and T. W. Huang, *EMAP 2008*, (2008)25, Taiwan, DOI:10.1109/EMAP.2008.4784220
21. S. C. Chang, T. C. Lin, and T. S. Li, *Journal of Nanomaterials*, 2014(2014)Article ID 690498.
22. W. Ma, C. Yang, X. Gong, K. Lee and A. J. Heeger, *Advanced Functional Materials*, 15(2005)1617.
23. A. Guerrero, P. Boix, L. F. Marchesi, T. Sanchis, F. C. Pereira and G. Garcia-Belmonte, *Solar Energy Materials & Solar Cells*, 100(2012)185.
24. P. E. Hopkinson, P. A. Staniec, A. J. Pearson, A. D. F. Dunbar, T. Wang, A. J. Ryan, R. A. L. Jones, D. G. Lidzey, and A. M. Donald, *Macromolecules*, 44(8)(2011)2908.
25. D. Chirvase, J. Parisi, J. C. Hummelen and V. Dyakonov, *Nanotechnology*, 15(9)(2004)1317.
26. W. H. Lee, S. Y. Chuang, H. L. Chen, W. F. Su and C. H. Lin, *Thin Solid Films*, 518(2010)7450.
27. G. Kalonga, G. K. Chinyama, M. O. Munyati and M. Maaza, *Journal of Chemical Engineering and Materials*, 4(7)(2013)93.
28. D. Chirvase, J. Parisi, J. C. Hummelen and V. Dyakonov, *Nanotechnology*, 15(9)(2004)1317.

© 2015 The Authors. Published by ESG ([www.electrochemsci.org](http://www.electrochemsci.org)). This article is an open access article distributed under the terms and conditions of the Creative Commons Attribution license (<http://creativecommons.org/licenses/by/4.0/>).